Available online at www.sciencedirect.com
SCIENCE DIRECT®
Journal of Computational Physics 188 (2003) 348–364
JOURNAL OF COMPUTATIONAL PHYSICS
www.elsevier.com/locate/jcp

Localization and spreading of contact discontinuity layers in simulations of compressible dissipationless flows

N.J. Zabusky *, S. Gupta, Y. Gulak

Laboratory for Visiometrics and Modeling, Department of Mechanical and Aerospace Engineering, and Center for Advanced Information Processing (CAIP) Center, Rutgers University, Piscataway, NJ 08855-8058, USA

Received 4 September 2001; received in revised form 23 October 2002; accepted 29 October 2002

Abstract

We introduce a systematic approach to examine the localization and width of contact discontinuity layers (CDLs) in simulations of the compressible Euler equations. We study the Piecewise Parabolic Method (PPM) [4] and WENO [3], by simulating a single diffusing or shock-accelerated CDL in 1D and 2D (inclined planar interface). Here the density jump η is greater or less than unity (i.e., fast/slow {f/s} and slow/fast {s/f}, respectively). We advocate a point-wise algorithm for width extraction when the flows are nearly-discontinuous. We examine the CDL localization under mesh refinement and the CDL width spreading at long times. We find that, PPM has an asymmetrically developing CDL width. PPM introduces an artificial steepening for the f/s case and a spreading width CDL for s/f $\propto t^{1/3}$. The median point of the interface depends on the order of accuracy r. For PPM, $r = 2$, it is located at a density, $(\rho_1 + 2\rho_2)/3$, consistent with analysis in [14]. For WENO, $r = 3$, (5th order accurate in smooth monotone regions) the width of the CDL increases as $t^{1/4}$, although there is a slight dependence on translation speed of the CDL. These observations are essential for establishing the validity of simulations of accelerated flows of high-gradient stratified and compressible media (Rayleigh–Taylor and Richtmyer–Meshkov environments), particularly for *reshock* configurations in 2D and 3D.

Keywords: Accelerated flows; Contact discontinuity localization; Contact discontinuity spreading; Richtmyer–Meshkov

1. Introduction

The long time evolution of interfacial domains between media of different density (or other intrinsic properties) is of fundamental importance in many fluid fields. In particular our interest is the turbulent mixing in the *accelerated inhomogeneous flow* or "*aif*" environment [15].

At present the foci of application for this environment (also called Richtmyer–Meshkov impulsive or Rayleigh–Taylor environment) are to inertial confinement (e.g., laser) fusion [9], supersonic combustion [5]

* Corresponding author. Tel.: +1-732-445-3124; fax: +1-732-445-5313.
E-mail address: nzabusky@caip.rutgers.edu (N.J. Zabusky).

0021-9991/03/$ - see front matter
doi:10.1016/S0021-9991(02)00045-1

or supernova and planetary nebula astrophysics [10]. In many cases the acceleration is produced by shock or blast waves. Simulations are usually done with finite volume or finite difference codes like PPM [4] or WENO [3], which are written for non-dissipative media. Many studies have examined order of accuracy and convergence of these methods (see [1] and references therein). However, they usually focus on properties of shocks and frequently omit a careful study of the localization and spreading of high-gradient density-stratified domains or contact discontinuity layers (CDL), as we call them. In fact, these are the essential locations for the turbulence which emerges at shear or vorticity bearing layers in shocked flows, a frequent occurrence at late time in these investigations.

Also there is the issue of the well posedness of the original non-dissipative formulation of the problem. Many have shown (e.g. [2,11]) that the ill-posed nature of the shock-interface problem manifests in the more rapid roll-up of the interface as one refines the mesh. This arises because the same circulation per unit length is being deposited by the shock on the interface while the roll-up time (or inverse vorticity) decreases with decreasing mesh size. Thus the interface becomes structured more quickly and develops very high curvature regions in a finite time. (Note an Atwood number of unity may be an exception [2].) Numerous ad hoc techniques are employed by investigators to modify their *subjective feeling* of an inappropriate evolution of the density discontinuities. These modifiers include contact "steepeners", artificial compression methods [3], dealiasing filters, and flux limiters. These modifiers operate in regions where the evolving circulation may be large.

Contact surfaces arise from the initial arrangement of matter in regions of different density or γ, the ratio of specific heats, (e.g., bubbles or clouds of materials in an ambient environment) or thru the formation of "triple" points where shocks of sufficient Mach number cross each other at finite angles. The spreading of regions of large gradients is controlled by diffusion processes – either physical or numerical. However, in two or higher dimensions, when vorticity (in thin layers) is associated with the high gradient regions the diffusion process is complicated by advective (mixing) effects and the region has a turbulent or "complex" behavior. This is particularly challenging if there are repeated shock interactions or re-accelerations of the CDL [8].

In this paper, we discuss the quantification of the localization and spreading of CDLs from numerical processes. We do this in one dimension and two dimensions for two codes, which are generic and popular at present: PPM (obtained from the Virginia Hydrodynamics group and based on [4]) and WENO [3].

1.1. Motivation

This work has its roots in the recent study by Samtaney and Zabusky [12] of the visualization and quantification of 2D simulations of a shock interacting with a planar inclined contact discontinuity as

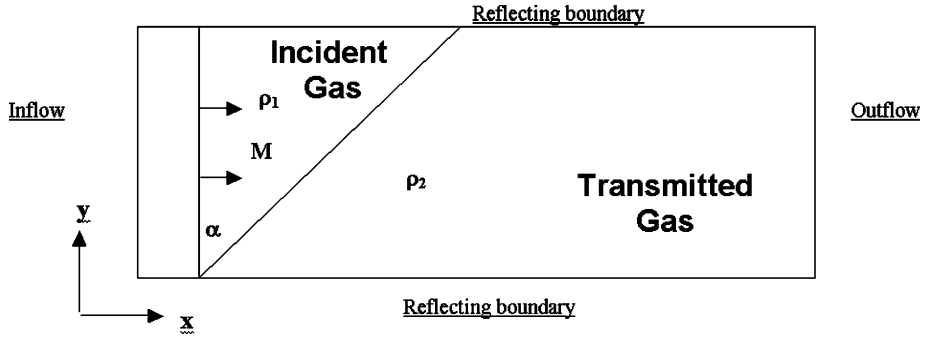

Fig. 1. Initial configuration of a shock of Mach number M moving to the right in ambient density ρ_1 and a planar inclined contact discontinuity (CD), followed by a region of density ρ_2.

shown in Fig. 1. They quantified high-gradient regions (shocks and contact discontinuities) by using a variant of an edge detection technique (corresponding to the zero crossing of the Laplacian of the density field) to obtain a contour. Samtaney et al. [12] have generalized this technique to 3D for the extraction of "*shocklets*".

To establish the validity of the method, Samtaney and Zabusky did a convergence study for the 1D problem of a shock ($M = 3.0$) interacting with a density discontinuity ($\rho_2/\rho_1 = 3.0$), which allows a simple exact solution. However, they found that the location of the contact discontinuity at $(1/2)(\rho_1 + \rho_2)$ as shown in Curve C of Fig. 2 (their Fig. 12.9) did not converge to the exact analytical location, when the contact discontinuity was extracted with the zero crossing of the second central difference of density, d^2r. In fact, as shown, the error under mesh refinement obeys a power law variation in mesh size.

Furthermore, in a recent study, for a weak shock ($M = 1.095$) interacting with a heavy gas (SF_6) cylinder, Gupta [6] observes an *asymmetry* in steepening of the upstream (f/s) and downstream (s/f) interfaces after passage of shock when using PPM. Fig. 3(a) shows a horizontal slice of the normalized *density gradient* near the axis at six different times *after* the shock has passed the cylinder. The increase of both gradients is caused by strong nearby vortex domains that arise from the roll-up of the deposited primary circulation. We see the upstream and downstream interfaces evolve asymmetrically.

The downstream (s/f) interface (marked by D*m*, where *m* is an integer) increases more rapidly since it is nearer to the vortex and the magnitude saturates because of numerical diffusion. The upstream (f/s) interface (marked by U*m*) is further from the vortex domain and continues to steepen and then saturates. This asymmetry slightly affects the evolution of global circulation, as shown in Fig. 3(b). The steady increase in circulation after primary vorticity deposition is due to "secondary" baroclinic generation arising from the *acceleration* produced by the strong vortex domains. This process is augmented by a density-gradient intensification and the asymmetric behavior of the f/s (upstream) and s/f (downstream) interface will affect the evolution of negative and positive circulations, respectively. This *vortex-accelerated* baroclinic deposition will be discussed more completely in a future publication.

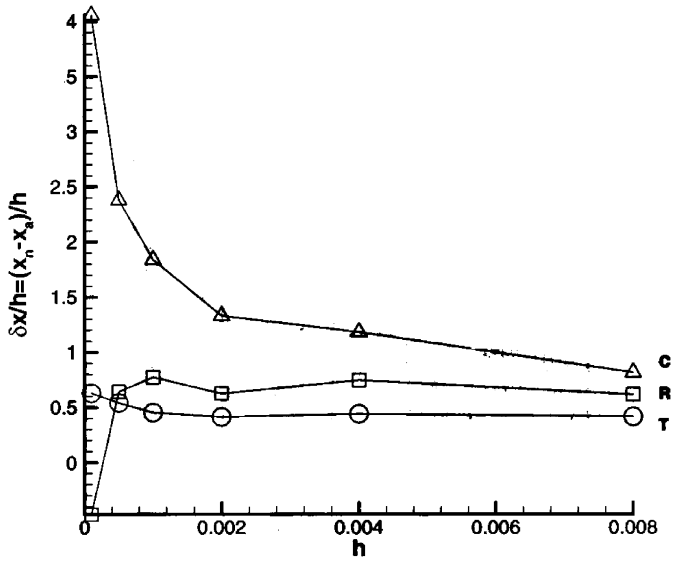

Fig. 2. Convergence study using the difference in the numerical and analytical locations of high gradient regions vs mesh size h. Here, an $M = 3.0$ shock interacts with a density discontinuity (CD, $\rho_2/\rho_1 = 3.0$) and yields a moving CD (C), upstream reflected shock (R), and downstream transmitted shock (T) (see [13]). The numerical location point for each discontinuity (T, R, and C) is at the zero crossing of the second central difference of the density.

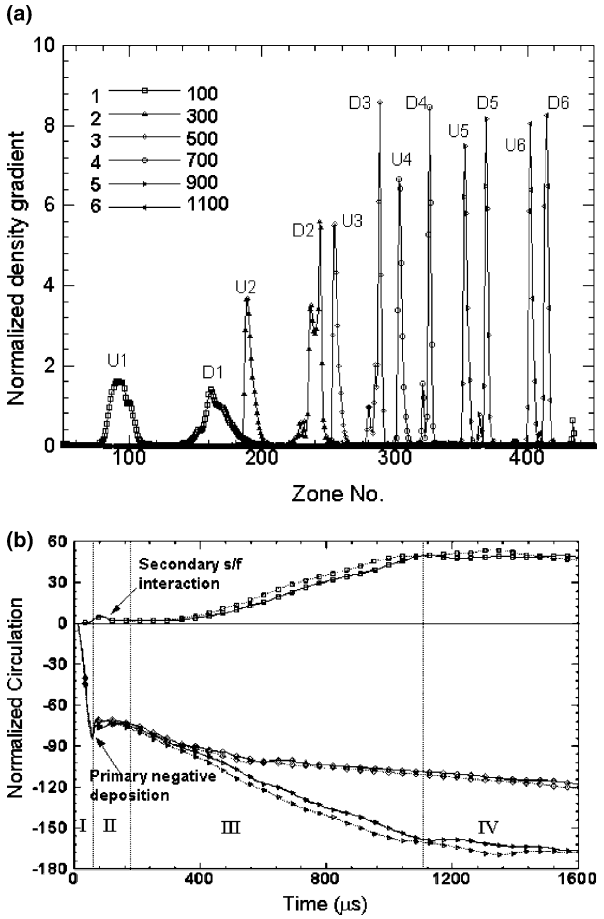

Fig. 3. Evolving normalized density gradient, $(\nabla\rho/\nabla\rho|_{0,\max})$ near the x-axis (along a horizontal slice at $j = 5$) after the passage of a $M = 1.095$ shock interacting with a cylinder of SF_6 in air. The two nearby peaks in gradient profile represent the upstream and downstream interface and are designated by "Um" and "Dm", respectively. Here m refers to the six times shown upper left. Fig. (b) shows the global positive (Γ_+), negative (Γ_-) and net (Γ_{net}) circulations as a function of time (tM) normalized by Mach number. Circulations are plotted for two *initial transition layer* widths. The evolution of circulation during the secondary baroclinic phase (III) is aided by the gradient intensification.

2. Continuum limits and linear differential approximation technique

To explain the non-convergent phenomenon observed by Samtaney and Zabusky [12], we use the elegant error analysis of Vorozhtsov and Yanenko [14], which employs the concept of continuum limits of discrete systems, or "Differential Approximations" introduced by Shokin [13]. First, consider the 1D Riemann problem for the Euler system

$$\frac{\partial U}{\partial t} + \frac{\partial \varphi(U)}{\partial x} = 0. \tag{1}$$

Here $U = (\rho, \rho u, \rho E)^{\mathrm{t}}$ and $\varphi(U) = (\rho u, p + \rho u^2, u(p + \rho E)^{\mathrm{t}}$. Here the total specific energy is $E = \varepsilon(p, \rho) + u^2/2$, and the internal energy ε is a prescribed equation of state. In our work we use,

$$\varepsilon = p/\rho(\gamma - 1) = RT/(\gamma - 1).$$

To examine the spreading of a CD we examine a simple problem given by the constant initial data

$$u(x,0) = u_0, \quad p(x,0) = p_0, \quad \rho(x,0) = \begin{cases} \rho_1, & x < x_0, \\ \rho_2, & x > x_0. \end{cases} \tag{2}$$

Thus, we reduce Eqs. (1) and (2) to the solution of a linear equation

$$\frac{\partial \rho}{\partial t} + u_0 \frac{\partial \rho}{\partial x} = 0. \tag{3}$$

Here $\mathrm{d}x/\mathrm{d}t = u_0$ is the characteristic along which the contact discontinuity propagates. The numerical algorithm and code approximates this $(1+1)$ partial differential equation with finite-difference methods, which can have an rth order of spatial accuracy. That is, the continuum limit (or differential approximation (DA)) obtained from a Taylor series expansion of the discretized version of Eq. (3) has the form

$$\frac{\partial \rho}{\partial t} + u_0 \frac{\partial \rho}{\partial x} = (-1)^{r+1} \mu_{r+1} \frac{\partial^{r+1} \rho}{\partial x^{r+1}}, \tag{4}$$

where only the leading term in a infinite series has been kept on the right-hand side, μ_{r+1} is a constant dependent on h, Δt, u_0, and p_0, where h and t_Δ are the spatial grid size and time step of the numerical algorithm, respectively. Note, an equation identical to this one, namely first order in time and $(r+1)$ order in space, was presented by Harten [7] in his discussion of the spreading of a discontinuity in the numerical solutions of a linear advection equation obtained by an rth order difference scheme. For first- and second-order methods, $r = 1$ and $r = 2$, the similarity solutions (given in [14]) corresponding to initial conditions (2) are, respectively

$$\rho(x,t) = 0.5(\rho_1 + \rho_2) + 0.5(\rho_2 - \rho_1)\mathrm{erf}(\xi), \tag{5}$$

where $\xi(x,t) = (x - x_0 - u_0 t)/(2\mu_2 t)^{1/2}$ and

$$\rho(x,t) = (2\rho_2 + \rho_1)/3 + (\rho_2 - \rho_1) \int_0^{\xi} \mathrm{Ai}(\xi')\, \mathrm{d}\xi', \tag{6}$$

Table 1
Density profiles for different runs

Figs.	Evolution	η or η^*	Vel (u_0 or M)	nD	α	C/r	h^*1000
5(a)	F	0.14	1.5	1	N/A	PPM/2	10,2,0.5
5(b)	F	0.14	1.5	2	0	PPM/2	10,2,0.5
5(c)	F	0.14	1.5	2	30	PPM/2	10,2,0.5
7(a)	F	7.0	1.5	1	N/A	PPM/2	10,2,0.5
7(b)	F	7.0	1.5	2	0	PPM/2	10,2,0.5
6(a)	S	0.142	1.5	1	N/A	PPM/2	10,2,0.5
6(b)	S	0.142	1.5	2	0	PPM/2	10,2,0.5
6(c)	S	0.142	1.5	2	10	PPM/2	10,2,0.5
8(a)	S	6.83	1.5	1	N/A	PPM/2	10,2,0.5
8(b)	S	6.83	1.5	2	0	PPM/2	10,2,0.5
10(a)	S	0.142	1.5	1	N/A	WENO/3	10,2,0.667
10(b)	S	6.83	1.5	1	N/A	WENO/3	10,2,0.667

where $\xi(x,t) = (x - x_0 - u_0 t)/(3\mu_3 t)^{1/3}$. Here

$$\mathrm{erf}(\xi) = \frac{2}{\sqrt{\pi}} \int_0^{\xi} \mathrm{e}^{-s^2}\,\mathrm{d}s$$

is the error function and $\mathrm{Ai}(s)$ is the oscillatory Airy function whose properties can be found in [17]. Although this analysis is valid only for linear equations we find below, excellent agreement with PPM ($r = 2$) and WENO ($r = 3$) non-linear codes. The WENO scheme, based on the rth-order accurate ENO scheme, is $(r+1)$th-order accurate in smooth monotone regions, although this is still not as good as the optimal order $(2r-1)$ [16].

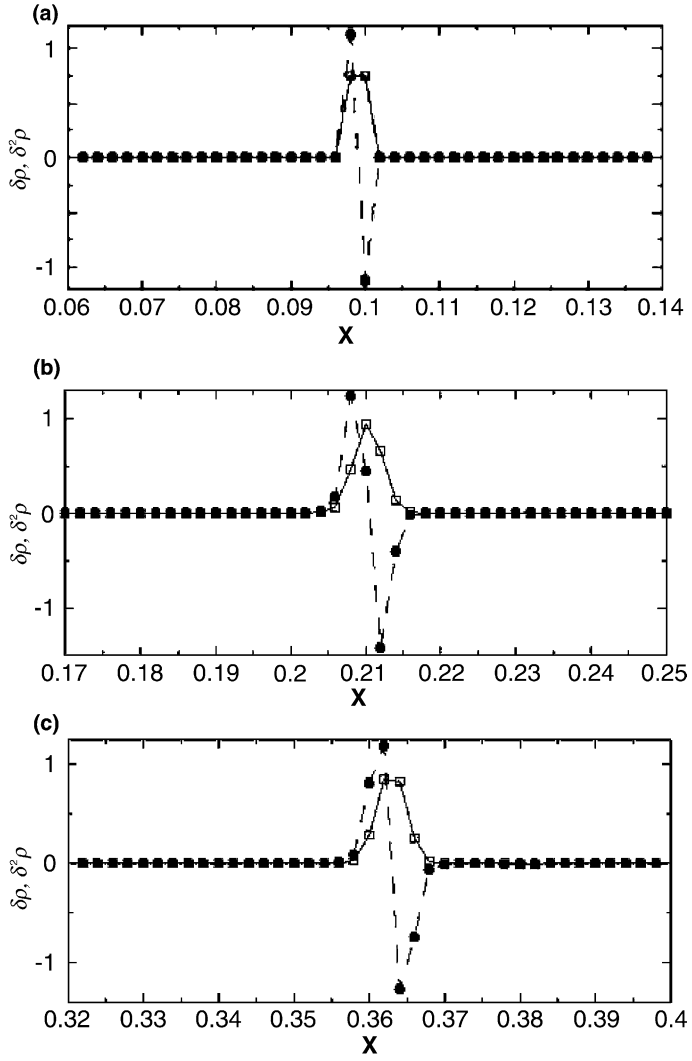

Fig. 4. Extraction procedure for the width of a CDL involves taking the difference of locations between maximum and minimum second central difference ($\delta^2\rho$). The width of contact discontinuity remains almost constant in f/s case (**F**, 1D). Solid line with squares is $\delta\rho$ and dashed line with black circles is $\delta^2\rho$ (a) $t = 0.0$, (b) $t = 0.27$, (c) $t = 0.6$.

3. Localization and spreading of a contact discontinuity

3.1. Evolution and extraction of a CDL

We examine and *quantify* the evolution of a CD layer (CDL), an *initial* density jump of finite small width O(h) in 1D and 2D. We examine two cases, designated as (**F**) and (**S**). In the former, the CDL evolves *freely* while translating with u_0 and in the later it is at rest and struck by a shock of Mach number M, entering from the left. The CDL may be an increase or decrease in density, i.e. ratio $\eta > 1.0$ and <1.0, {"fast/slow" (f/s) or "slow/fast" (s/f)}, respectively. In this study, we use $\rho_1 = 1$ and $\rho_2 = 0.14$ for the (s/f) case and $\rho_1 = 1$ and $\rho_2 = 7.0$ for the f/s case. (For the **S** case, the density ratio, η^* is that after the shock has passed.) The 2D runs are for the clockwise-inclined planar interfaces at α degrees to the vertical, as shown in Fig. 1. For $\alpha = 0$ in 2D, we examine how a 2D code computes an initially 1D initial condition. For 2D runs we, examine only the horizontal slice, which is located midway between the two horizontal boundaries.

The simulations are done with PPM ($r = 2$) and WENO ($r = 3$). WENO uses a third-order accurate Runge–Kutta method [3]. Table 1 summarizes the runs.

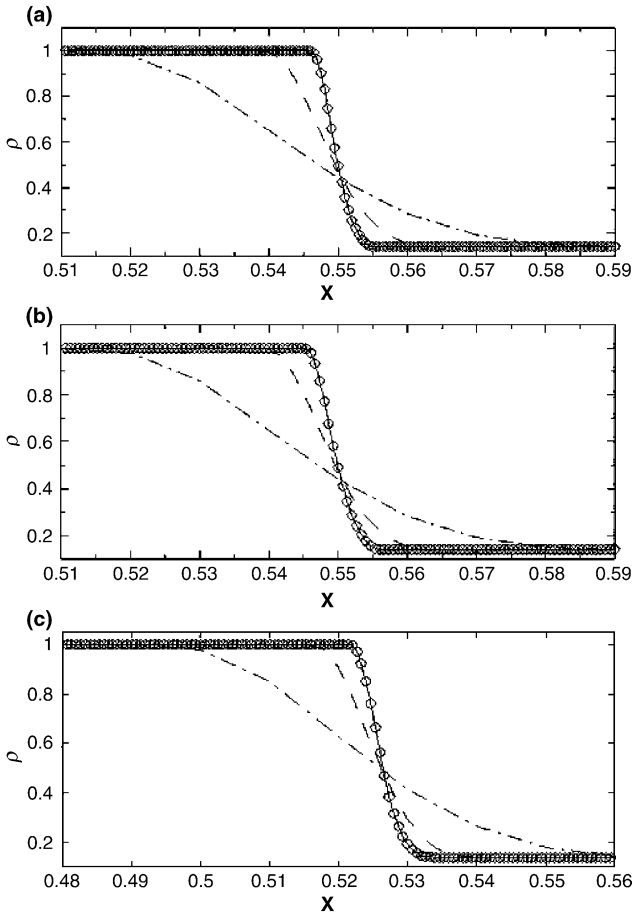

Fig. 5. Density profile at $t = 0.3$ for (**F**), a diffusing contact with initial speed $u_0 = 1.5$ and $\eta = 0.14$ and varying resolutions. Solid line with circles is the highest resolution 0.0005 (- - -) and (-···-) are 0.002 and 0.01, respectively. (a) 1D, (b) 2D, $\alpha = 0$, (c) 2D, $\alpha = 30°$.

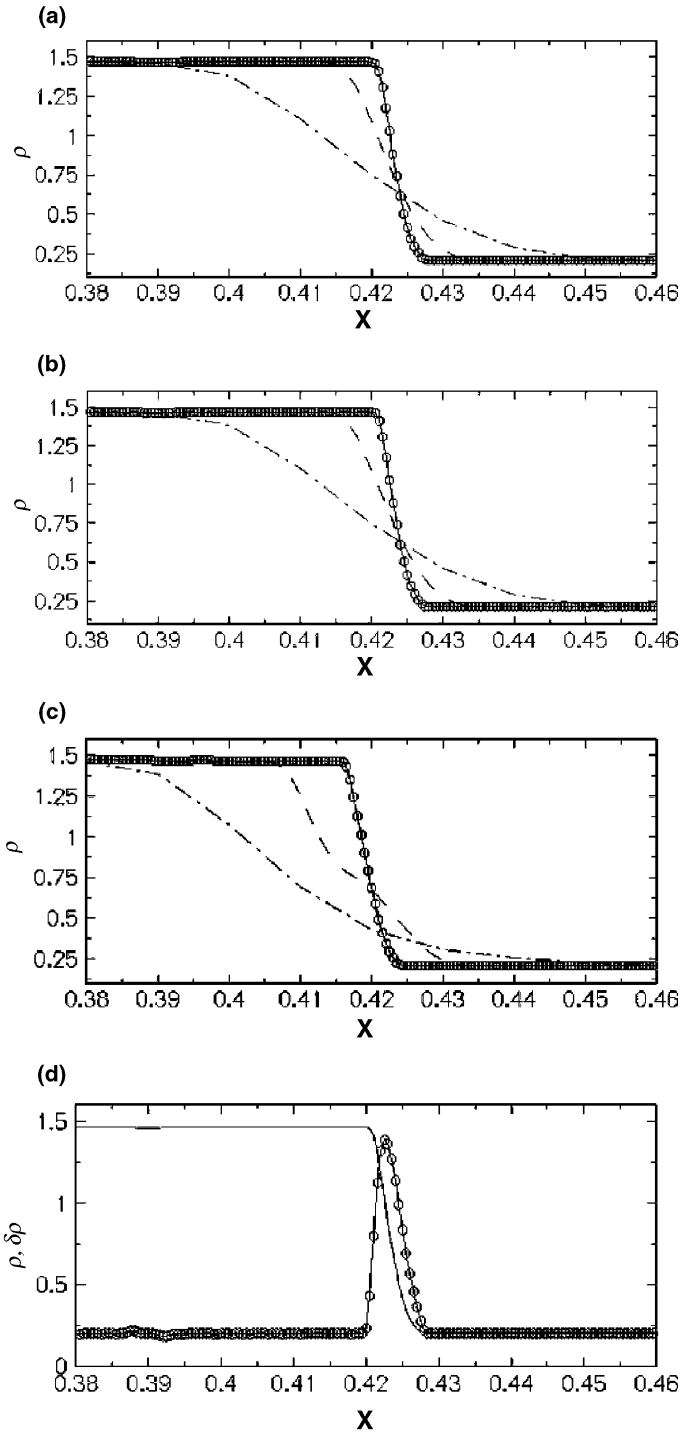

Fig. 6. Density profiles at $t = 0.3$ for a Mach 1.5 shock–contact interaction (**S**) and $\eta = 0.14$ and varying resolutions. The solid line with open circles is the highest resolution 0.0005 and (- - -) and (·····) are 0.002 and 0.01, respectively. (a) ρ, 1D (b) ρ, 2D, $\alpha = 0$, (c) ρ, 2D, $\alpha = 10$, (d) ρ and $\delta\rho$, 1D.

First, we examine the graphs of density to *localize* of the point of "transition" of the CDL under mesh refinement. Next we examine the *spreading* of the CDL. The width of the CDL is defined as the interval between extrema of second central difference of density. (This width is almost half the distance between positions where $\delta\rho > \delta\rho_{\text{thresh}}$.) We use an accurate point-wise algorithm to extract this width, as described in Appendix A. For example, Fig. 4 shows the first and second central difference of the density function at $t = 0$, 0.27 and 0.6 for a 1D f/s ($\eta = 7.0$) case. Note at $t = 0$, the interval between extrema of the 2nd central difference is h.

3.2. Localization of a CDL with PPM and WENO under mesh refinement

We examine how ρ evolves with varying resolutions – a range of 20, from 0.01 to 0.0005. Figs. 5(a)–(c) (**F**, $u_0 = 1.5$, 1D, 2D ($\alpha = 0$ and $\alpha = 30$), $\eta = 0.14$) show that as the resolution increases all the curves intersect nearly at the same location, $\rho = 0.44$. This is very good agreement with Eq. (6) for a second-order scheme which predicts the intersection point as 0.43 for densities used. We recommend this intersection point as a valid approximation in 1D to the true location of the contact discontinuity. This point is also close to the location where $\delta^2\rho = 0$. Similarly, for case (**S**) ($M = 1.5$ and $\eta = 0.14$) , the results in Figs. 6(a) and (b) in 1D and 2D ($\alpha = 0$) are 0.625 and 0.63, respectively, in close agreement to the analytical value, 0.63 (where post-shock densities are used). In Fig. 6(c) for finite angle ($\alpha = 10$), we see moderately good agreement, 0.665, with the predicted value for the two highest resolutions.

Fig. 6(d), for the **S**, $M = 1.5$ case in 1D shows an *asymmetry* in $\delta\rho$, which is a manifestation of the property of the Airy function (as discussed in detail in [14], Sec. 4.1.2). The numerical algorithm has suppressed the oscillations associated with the Airy function and this does not seem to affect the convergence of the CDL localization under mesh refinement.

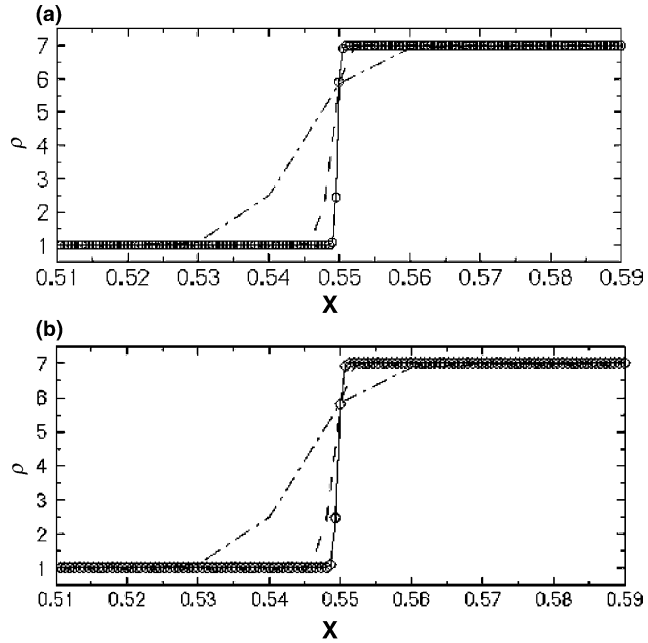

Fig. 7. Density profile at $t = 0.3$ for a diffusing contact (**F**) with initial speed $u_0 = 1.5$ and $\eta = 7.0$ and varying resolutions. Solid line with circles is the highest resolution 0.0005 and (- - -) and (-·-·-) are 0.002 and 0.01, respectively. (a) 1D, (b) 2D, $\alpha = 0$.

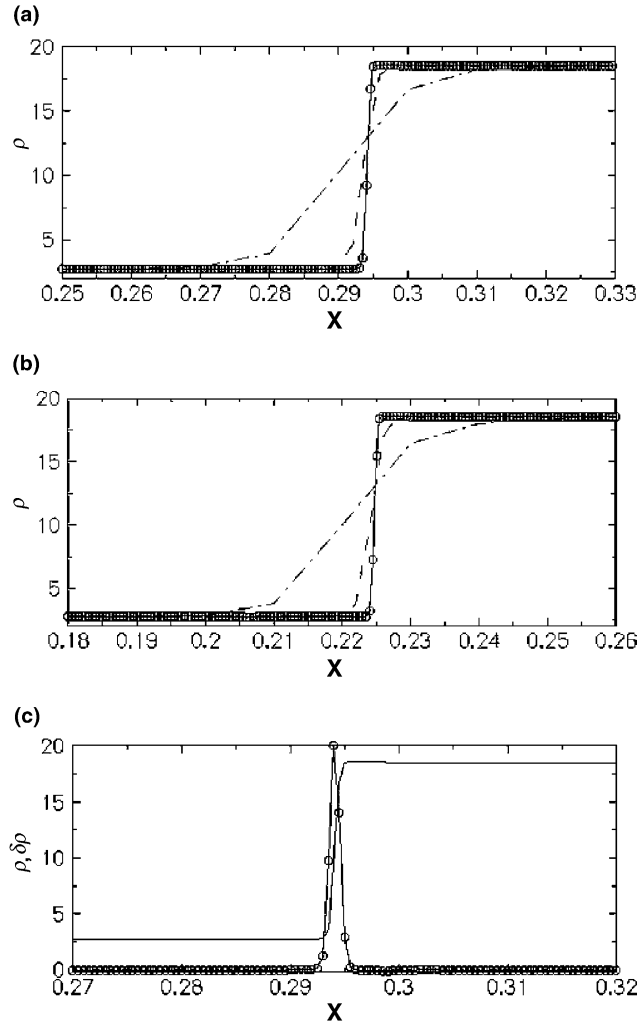

Fig. 8. Density profiles at $t = 0.3$ for a Mach 1.5 shock–contact discontinuity (**S**) with $\eta = 7.0$ and varying resolutions. The solid line with open circles is the highest resolution 0.0005 and (- - -) and (-···-) are 0.002 and 0.01, respectively. (a) ρ, 1D, (b) ρ, 2D, $\alpha = 0$, (c) ρ and $\delta\rho$, 1D.

Figs. 7(a) and (b) **F**, $M = 1.5$, $\eta = 7.0$ case shows density profiles. The different resolutions intersect at $\rho = 5.75$, reasonably close to the analytical value of $\rho = 5$. Note in Figs. 4(b) and (c) (for this case) that PPM maintains a width of one or two intervals for the CDL, as we will discuss below in Fig. 13. This is evident from the steeper density profiles in this case as compared to the s/f case in Fig. 5.

Figs. 8(a) and (b) for the **S**, $M = 1.5$, $\eta = 7.0$ case shows similar good results. The intersection point for the curves is 13.0 and 13.5, respectively, whereas the analytical value for the after shock densities is 13.27. In Fig. 8(c), the width of the CDL is *always* one or two mesh intervals and the asymmetry is barely noticeable. Note, Balsara and Shu [3] simulated four translating profiles with PPM with a steepener operating and also noted an asymmetry for one triangular shaped profile (their Fig. 1(d), left) of four studied. However, they did not comment on this asymmetry since their study was not focused on evolving CDLs.

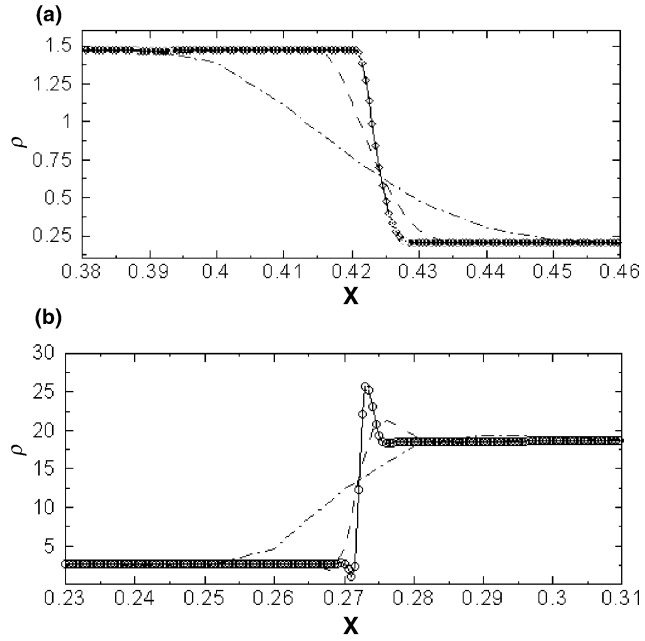

Fig. 9. Density profiles at $t = 0.3$ for a $M = 1.5$ shock–contact discontinuity (**S**) and varying resolutions. The PPM scheme is used without the van Leer limiter. The solid line with open circles is the highest resolution 0.0005 and (- - -) and (·····) are 0.002 and 0.01, respectively. (a) ρ, s/f ($\eta = 0.14$), (b) ρ, f/s case ($\eta = 7.0$).

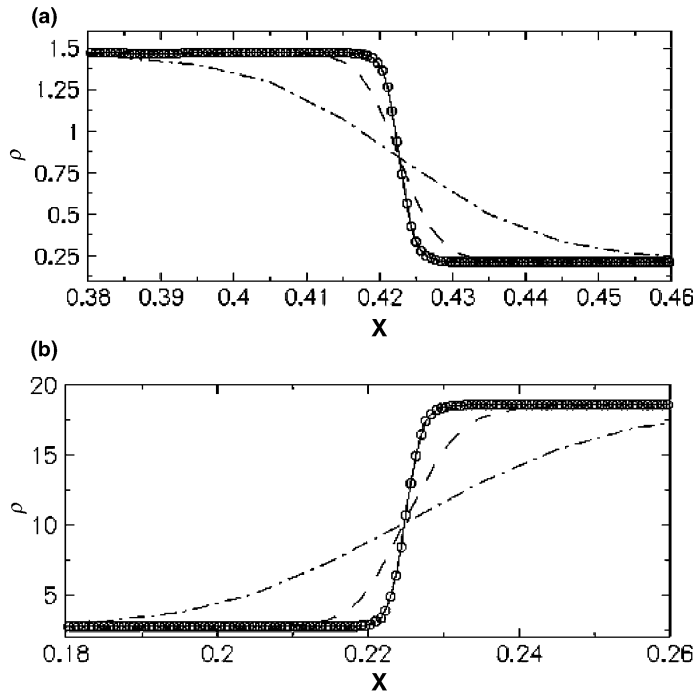

Fig. 10. Density profiles at $t = 0.3$ for shock–contact interaction (**S**) with $M = 1.5$ using the WENO ($r = 3$) code. Solid line with circles represents highest resolution 0.000667 and (- - -) and (·····) are 0.002 and 0.01, respectively. (a) ρ, s/f ($\eta = 0.14$), (b) ρ, f/s ($\eta = 7.0$).

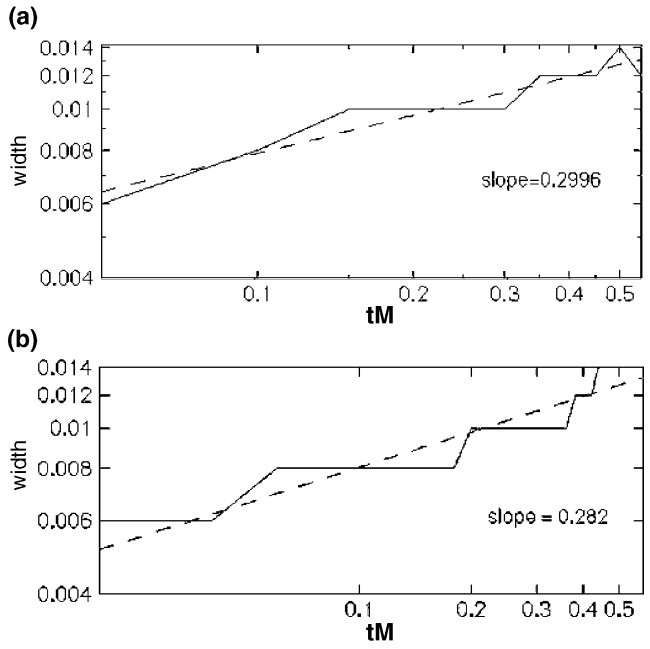

Fig. 11. Growth of width of a CDL for (**F**) and $u_0 = 1.5$ for $\eta = 0.14$. The curve is plotted for a resolution of 0.002. (a) 1D, (b) 2D, $\alpha = 0$.

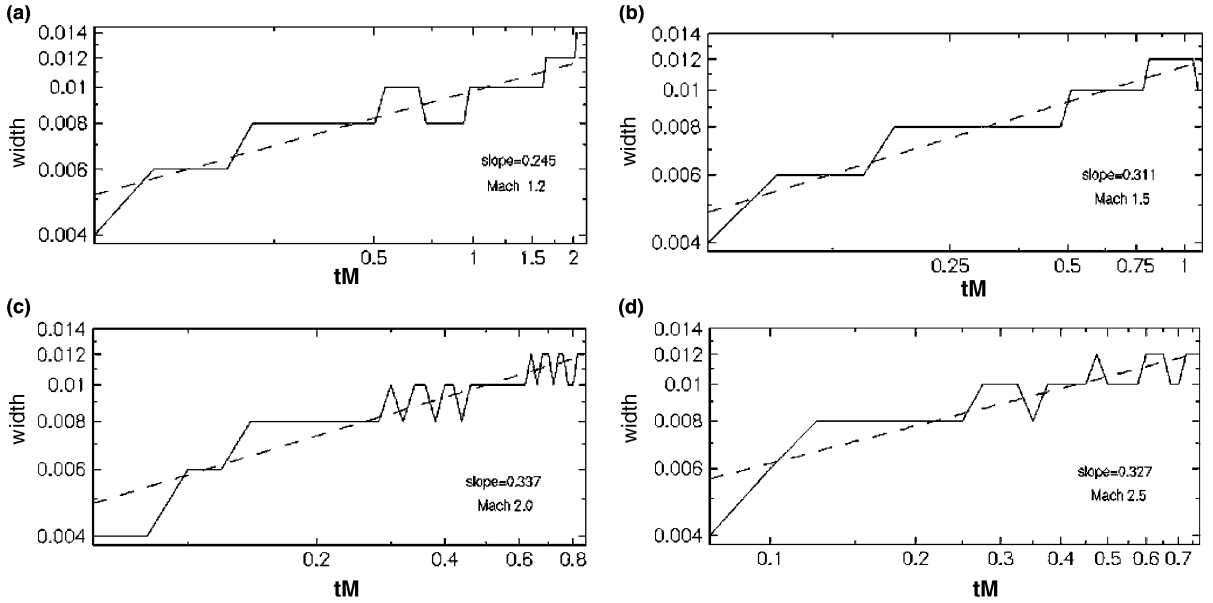

Fig. 12. Growth of width of a CDL for (**S**) and $\eta = 0.14$, 1D case. $U_0^* \Delta t$ is constant where U_0^* is the velocity of the CDL after the shock has passed. (a) $M = 1.2$, (b) $M = 1.5$, (c) $M = 2.0$, (d) $M = 2.5$.

The PPM code used contains no explicit steepener. However, the van Leer limiter (Eq. (1.8) in [4]) that is used to obtain monotonicity leads to larger gradients. To examine this limiter effect, we did 1D (**S**) at $M = 1.5$ *without* this limiter for s/f ($\eta = 0.14$) and f/s ($\eta = 7.0$) ratios as shown in shown in Figs. 9(a) and (b), respectively. We observe a loss of monotonicity near the contact discontinuity only in the latter. The density profile widths are the same as with a limiter, namely the f/s case is steeper than s/f case.

Figs. 10(a) and (b) for WENO ($r = 3$) (**S**), $M = 1.5$, $\eta = 0.14$ and $\eta = 7.0$, respectively shows convergence to the midpoint. The points of intersection are 0.85 (s/f) and 10.0 (f/s), respectively.

3.3. Spreading of a CDL with PPM and WENO under mesh refinement

The width of the CDL is obtained automatically from 1D data sets by a point-wise algorithm described in Appendix A. The algorithm extracts density jumps by searching for nearby opposite-signed values of extrema of the second central difference of density and then eliminates shocks. The variation in CDL width

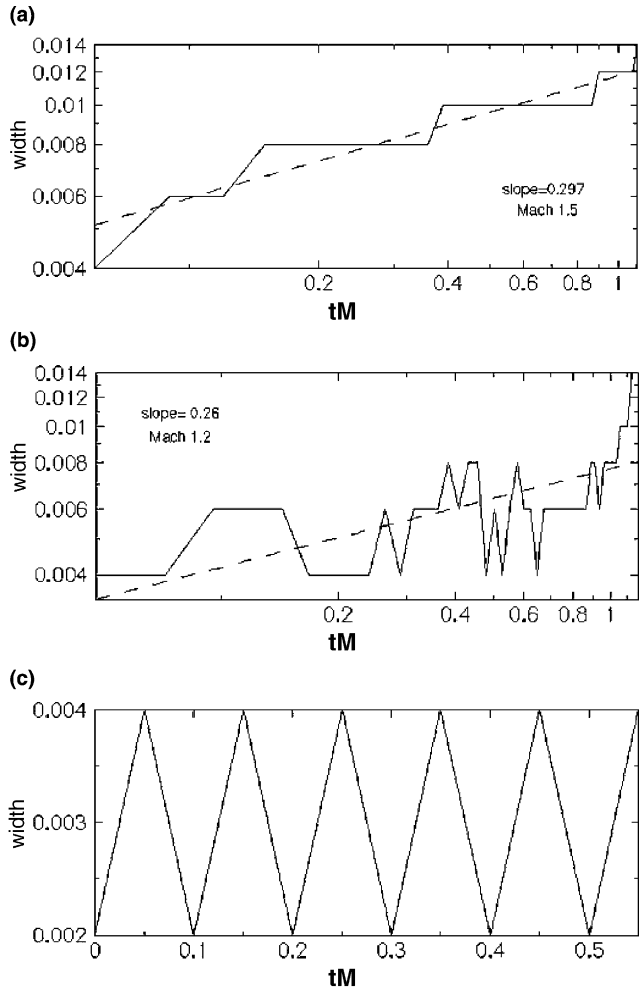

Fig. 13. Growth of width of a CDL for (**S**). (a) $M = 1.5$, $\eta = 0.14$, 2D, $\alpha = 0$. (b) $M = 1.2$, $\eta = 0.14$ 2D, $\alpha = 10$. (c) $M = 1.5$, $\eta = 7.0$, 1D. The curves are plotted for a resolution of 0.002.

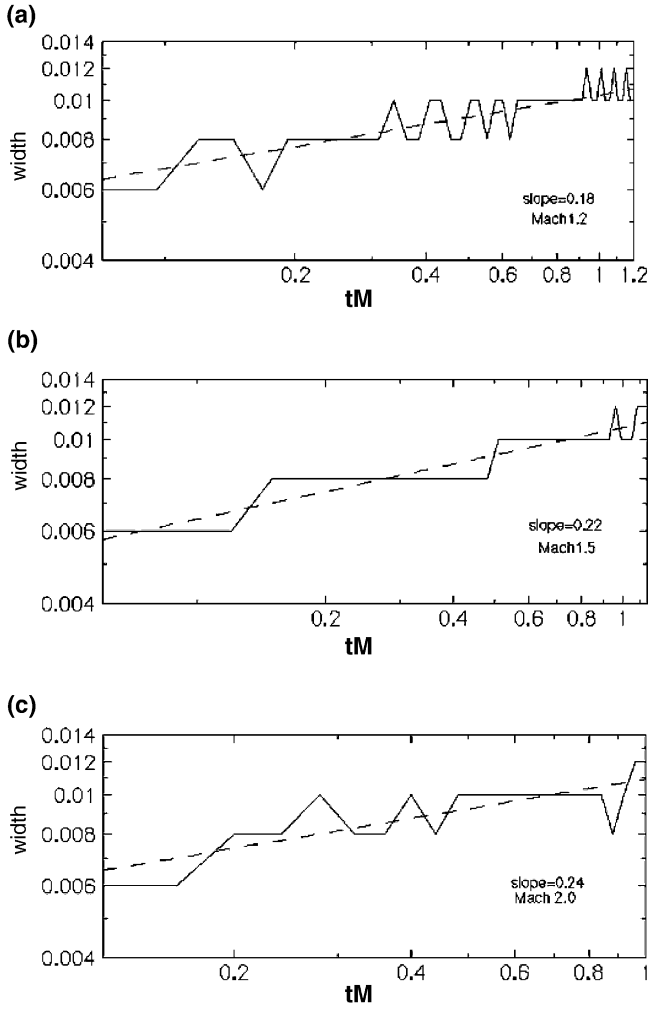

Fig. 14. Growth of width of a CDL for (**S**) and $\eta = 0.14$, 1D using WENO ($r = 3$). (a) $M = 1.2$, (b) $M = 1.5$, (c) $M = 2.0$.

is plotted in Figs. 11(a) and (b). for **F**, with $\eta = 0.14$ in 1D and corresponds to Figs. 5(a) and (b). The width begins at 3 mesh intervals and rises to a maximum of seven intervals. The power law slope is 0.30 and 0.28, respectively, close to the theoretical value of 0.33. These results were obtained with TECPLOT using a least squares fit to the function $w = \beta t^{\mathrm{p}}$ with 35–40 data points in the interval. Note the first curve is not monotonic (a process seen later) because of the sensitivity of the extraction scheme.

In Figs. 12(a)–(d) for **S** and corresponding to Fig. 6(a) for s/f we see a more oscillatory behavior in width growth. This phenomenon is associated with the interaction of the PPM simulation code and the point-wise extraction code. In essence, there is an oscillation over one grid interval before a steady plateau is reached. For Mach numbers, 1.2, 1.5, 2.0 and 2.5, the exponents are "p" are 0.25, 0.31, 0.34 and 0.33, respectively. (Note these results were obtained with identical CFL numbers, i.e., for increasing shock speed the time step was decreased.) At present we are unable to explain the slight increase of exponent with M.

In Fig. 13(a) corresponding to Fig. 6(b) (**S**, $\eta = 0.14$) the exponent is 0.3. In Fig. 13(b), corresponding to Fig. 6(d) (**S**, $\eta = 0.14$), the exponent is 0.26, a result of the complexity discussed above.

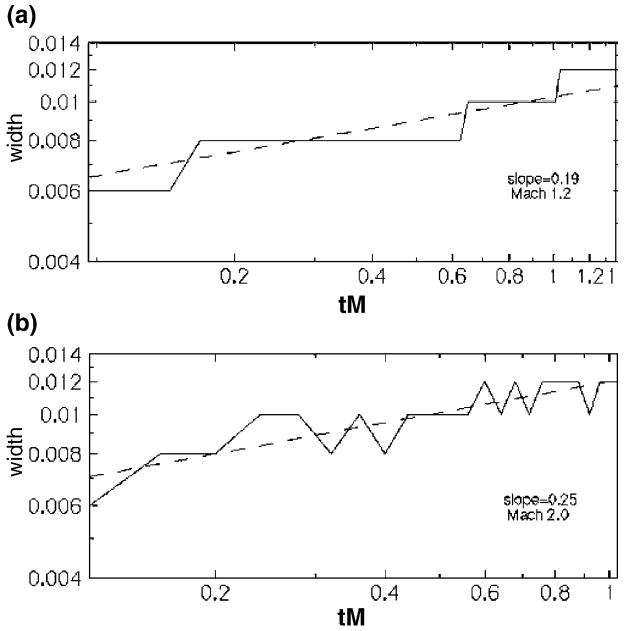

Fig. 15. Growth of width of a CDL for (**S**), $\eta = 7.0$, 1D using WENO ($r = 3$). (a) $M = 1.2$, (b) Mach 2.0.

Table 2
Spreading rates for different runs

Figs.	Evolution	η or η^*	Vel (U_0 or M)	nD	α	C/r	Exponent (p)
11(a)	F	0.14	1.5	1	N/A	PPM/2	0.2996
11(b)	F	0.14	1.5	2	0	PPM/2	0.282
13(c)	F	7.0	1.5	1	N/A	PPM/2	Oscillating
12(a)	S	0.142	1.2	1	N/A	PPM/2	0.245
12(b)	S	0.142	1.5	1	N/A	PPM/2	0.31
12(c)	S	0.142	2.0	1	N/A	PPM/2	0.337
12(d)	S	0.142	2.5	1	N/A	PPM/2	0.327
13(a)	S	0.142	1.5	2	0	PPM/2	0.297
13(b)	S	0.142	1.2	2	10	PPM/2	0.26
14(a)	S	0.142	1.2	1	N/A	WENO/3	0.18
14(b)	S	0.142	1.5	1	N/A	WENO/3	0.22
14(c)	S	0.142	2.0	1	N/A	WENO/3	0.25
15(a)	S	6.83	1.2	1	N/A	WENO/3	0.19
15(b)	S	6.83	2.0	1	N/A	WENO/3	0.25

In Fig. 13(c), corresponding to Fig. 7(a), (**F**, $\eta = 7.0$), the width *oscillates between one or two intervals*. We also find this phenomenon of narrow oscillations over the smallest intervals for (**S**) and $\eta > 1$.

Figs. 14(a)–(c) (**S**, $\eta = 0.14$, 1D) shows the growth of the CDL at varying Mach number for WENO ($r = 3$) code. The exponent ranges from 0.18 to 0.24, reasonably close to analytical result of 0.25. Fig. 15(a) and (b) (**S**, $\eta = 7.0$, 1D) shows that WENO third-order code does not show the oscillatory behavior of width function as does PPM (see Fig. 13(c)) for f/s case. The value of exponent in this case ranges from 0.19 to 0.25. Table 2 summarizes the spreading rates for different runs. In both PPM and WENO ($r = 3$), exponents are smaller for lower Mach numbers and converge towards the analytical value at as we increase the Mach number.

4. Discussion

We have presented a systematic approach to quantifying the evolution of a 1D CDL. We have used the second central difference approximation to the second derivative for extraction. We have applied these to inviscid schemes, PPM ($r = 2$) and WENO ($r = 3$), for simulations of ideal contact discontinuities that are freely diffusing (case **F**) or diffusing after shock passage (**S**). For these codes, our results on the localization of the CDL median point agree very well with analytical results based on a linear approximation to the truncation error in 1D [13] (when the CDL does not bear vorticity). For CDL spreading: a linearly translating interface, which is freely diffusing (**F** and $\eta < 1$) the temporal exponent of the extracted "width" varies from 0.25 to 0.33 for PPM (close to the analytical result of 0.33). However, for PPM we have found asymmetries in spreading in f/s case. That is, for $\eta < 1$, the CDL spreads as a power law whereas for $\eta > 1$, the width oscillates between one or two grid intervals. The WENO ($r = 3$) code does not have this asymmetry. The observed gradient intensification (artificial compression) in the PPM f/s case is still not understood.

This asymmetry phenomenon in PPM or other codes that employ an ad hoc "artificial compression" procedure will prove troublesome in realistic 2D and 3D problems where "re-acceleration" or "re-shock" phenomena occur at later times, in particular the important "mixing" epochs when the vorticity bearing interface (which are CD layers) are becoming turbulent.

Acknowledgements

This work has been supported by Rutgers University and in part by the Department of Energy (Grant DE-FG02-98ER25364) under Dr. Daniel Hitchcock. We acknowledge the use of the PPM code from the numerical astrophysics group at the University of Virginia (http://wonka.physics.ncsu.edu/pub/VH-1/VH-1_guide.html). We acknowledge the use of WENO codes from Dr. R. Samtaney of Princeton Plasma Physics Laboratory. He assisted us in their use and made valuable comments on an early manuscript. We acknowledge correspondence with E. Vorozhtzov on the historical context of diffusive spreading of discontinuous interfaces.

Appendix A. Extraction procedure for the width of a CDL

To obtain a measure for the *width* of the CDL automatically, we use a variation of the "edge detection" technique as described in [11]. We use the second central difference approximation to ρ_{xx}, $\delta^2\rho_i = \rho_{i+1} - 2\rho_i + \rho_{i+1}$. (For the 2D runs, we take a single slice, midway between the horizontal boundaries). We search the 1D domain for the largest nearby max and min of $\delta^2\rho_i$ and the interval between them is defined to be the *width*. For cases where shocks are present, we examine this interval after the shock has passed the interface and use the pressure jump and $\nabla \cdot \mathbf{u}$ as cost functions for excluding shocks and other noise. (Note, the pressure jump across the interval (normalized by the mean pressure) is less than a threshold $\mathrm{d}p_{\mathrm{thresh}}$ and $|\nabla \cdot \mathbf{u}| < |\nabla \cdot \mathbf{u}_{\mathrm{thresh}}|$, where $\mathrm{d}p_{\mathrm{thresh}}$ and $\nabla \cdot \mathbf{u}_{\mathrm{thresh}}$ are 0.1 and 0.025, respectively, of the value across the single large shock in our problem.)

References

[1] J. Comput. Phys. 169 (2) (2001) (This is a special volume on multiphase flows that examines the motion of the interfaces).
[2] G. Baker, R. Caflisch, M. Siegel, Singularity formation during Rayleigh–Taylor instability, J. Fluid Mech. 252 (1993) 51–78.

[3] D.S. Balsara, C.W. Shu, Monotonicity preserving weighted essentially non-oscillatory schemes with increasingly high order accuracy, J. Comput. Phys. 160 (2000) 405–452, The authors discuss the artificial compression method (ACM) and the role of ACM in preserving the order of accuracy for practical problems.
[4] P. Collella, P.R. Woodward, The Piecewise Parabolic Method (PPM) for gas-dynamical simulations, J. Comput. Phys. 54 (1984) 174–201.
[5] E. Curran, W. Heiser, D. Pratt, Fluid phenomenon in scramjet combustion systems, Annu. Rev. Fluid Mech. 28 (1996) 323–360.
[6] S. Gupta, Shock interactions with density inhomogeneities: simulation, validation, visualization and quantification, Masters Thesis, Department of Mech. and Aero. Eng., Rutgers University, 2002. Available from <www.caip.rutgers.edu/~sgupta/Thesis.pdf>.
[7] A. Harten, The artificial compression method for computation of shocks and contact discontinuities: I. Single conservation laws, Commun. Pure Appl. Math. 30 (1977) 611–638.
[8] A. Kotelnikov, J. Ray, N. Zabusky, Vortex morphologies on reaccelerated interfaces: visualization, quantification and modeling of one-and-two mode compressible and incompressible environments, Phys. Fluids 12 (2000) 3245–3264.
[9] J. Lindl, Development of the indirect drive approach to inertial confinement fusion and the target physics for ignition and gain, Phys. Plasmas 2 (1995) 3933–4024.
[10] B. Remington, D. Arnett, Intense lasers, in: Proc. 2nd Int. Workshop Lab. Astrophys., 1999.
[11] R. Samtaney, D. Pullin, On initial value and self-similar solution of the compressible Euler equations, Phys. Fluids 8 (1996) 2650–2655.
[12] R. Samtaney, N.J. Zabusky, High gradient compressible flows: visualization, feature extraction and quantification, in: T.T. Lim, A. Smith (Eds.), Flow Visualization: Techniques and Examples, Imperial College Press, 1999.
[13] Yu.I. Shokin, The Method of Differential Approximation, Springer, Berlin, 1983.
[14] V. Vorozhtzov, N.N. Yanenko, Methods for the Localization of Singularities in Numerical Solutions of Gas Dynamics Problems, Springer, Berlin, 1990.
[15] N.J. Zabusky, Vortex paradigm for accelerated inhomogeneous flows: visiometrics for the Rayleigh–Taylor and Richtmyer–Meshkov environments, Annu. Rev. Fluid Mech. 31 (1993) 495–536.
[16] G.-S. Jiang, C.-W. Shu, Efficient implementation of weighted ENO schemes, J. Comput. Phys. 126 (1996) 202–228.
[17] M. Abramowitz, I.A. Stegun (Eds.), Handbook of Mathematical Functions with Formulas, Graphs, and Mathematical Tables, National Bureau of Standards, 1972.